PERGAMON

Journal of Structural Geology 21 (1999) 23–37

JOURNAL OF STRUCTURAL GEOLOGY

Transtensional faulting patterns ranging from pull-apart basins to transform continental margins: an experimental investigation

Christophe Basile[a,*], Jean Pierre Brun[b]

[a]*Laboratoire de Géodynamique des Chaînes Alpines, CNRS UPRES-A 5025, 15 rue Gignoux, 38031 Grenoble Cedex, France, E-mail: cbasile@ujf-grenoble.fr*

[b]*Geosciences Rennes, CNRS UPR 4661, Campus de Beaulieu, 35042 Rennes Cedex, France, E-mail: Jean-Pierre.Brun@univ-rennes1.fr*

Received 28 January 1998; accepted in revised form 27 August 1998

Abstract

Seventeen small-scale experiments were performed to study the deformation induced in brittle–ductile models by a releasing stepover between two transform faults, and by intersection between transform and divergent plate boundaries. In both cases, faulting depends on the rheological layering (presence and strength of a ductile layer at depth) and the width of the basal stepover. Successive types of pull-apart basins are observed in the first set of experiments, which are compared with natural examples. Firstly, a lazy Z-shaped basin appears, which is bounded by Y faults above transform boundaries and R faults propagating from each corner of the stepover. Then, R′ faults replace R faults, leading to a rhomb-shaped graben. At every stage, the basin length-to-width ratio remains between 2.2 and 3.8, suggesting that scale independence of pull-apart basins is related to the geometrical shape of bounding faults. In a second set of experiments, deformation at the end of a transform boundary is characterized by a horsetail splay bounding a divergent basin. Within the horsetail splay, block tilting and block rotation about vertical axes lead to a surface slope perpendicular to the slope of the divergent basin, a feature that can be compared with marginal ridges at transform margins.

1. Introduction

Many sedimentary basins are tectonically controlled by an association of strike-slip and normal faults (e.g. Christie-Blick and Biddle, 1985; Sylvester, 1988). They result from various geodynamic environments at plate boundaries or within plates. At plate boundaries, such basins range from pull-apart basins in transform fault stepovers (Freund, 1974; Mann et al., 1983) to intersections of transform and divergent plate boundaries at transform continental margins (Mascle and Blarez, 1987) or at mid-ocean ridges (Fox and Gallo, 1984). They provide evidence for transtension, i.e. a combination of strike-slip and extensional components in the deformation. These basins are not only characterized by associations of strike-slip faults and normal faults, but also display block tilting and block rotation around a vertical axis.

In the present paper, we summarize two series of laboratory experiments on analogue models that focus on the crustal-scale effects of transform fault stepovers and on intersections between transform and divergent plate boundaries. Experimental results are compared to natural examples such as the pull-apart basins of the Dead Sea transform and the Ivory Coast–Ghana transform margin.

2. Experimental apparatus and materials

The experimental apparatus is of the Riedel box type, where the displacement of a plastic sheet produces two types of plate boundaries at the base of the model: a divergent boundary perpendicular to the displacement, and a right-lateral transform boundary parallel to the displacement (Fig. 1).

A first set of experiments addresses the formation and evolution of pull-apart basins (PA in Table 1). Two transform boundaries are linked by a perpendicu-

* Corresponding author.

0191-8141/99/$ - see front matter
PII: S0191-8141(98)00094-7

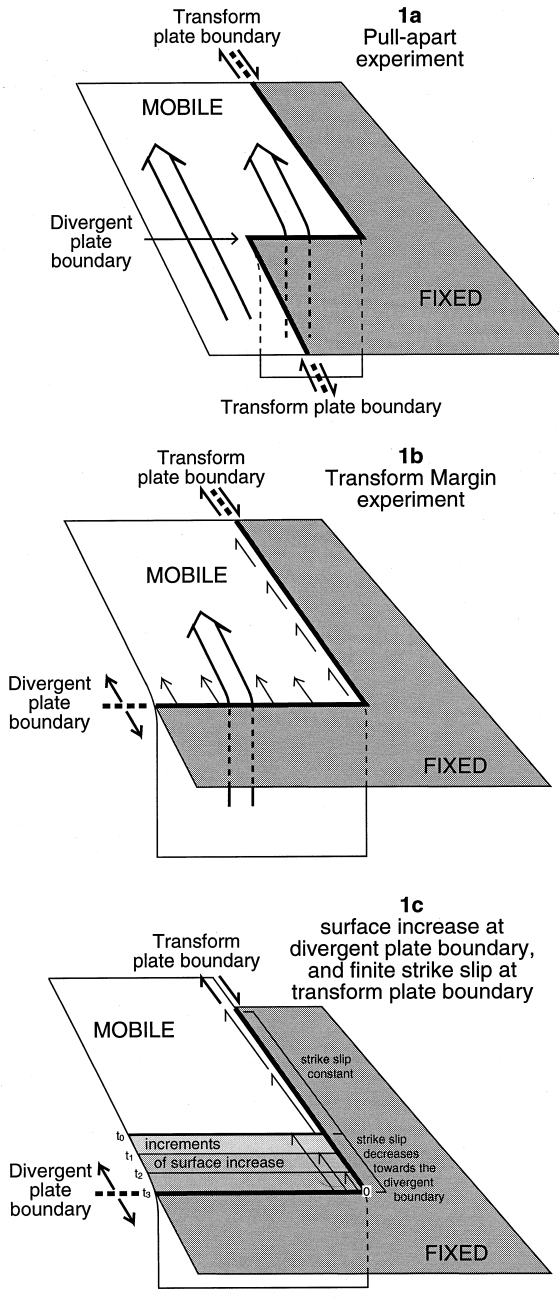

Fig. 1. Experimental apparatus used for PA (pull-apart, a) and TM (transform margin, b) experiments. Kinematic constraints induced by this apparatus are shown in (c).

lar releasing step (divergent boundary) (Fig. 1a). This apparatus allows the study of transform fault connections in the stepover domain. A second set of experiments addresses the deformation at the intersection between transform and divergent plate boundaries (transform margin case, TM in Table 1). The divergent boundary is long enough to develop divergent structures independently, and has a single connection to the transform boundary (Fig. 1b). In contrast to the previous apparatus, the connection between transform faults cannot occur.

In both arrangements the plate boundaries are fixed and cannot move during the experiment. Only one plate is mobile at the divergent plate boundary, inducing an asymmetric basin above the divergent boundary (except in experiment PA8, where both plates are pulled apart symmetrically) (Allemand et al., 1989; Allemand and Brun, 1991; Tron and Brun, 1991). The displacement of the mobile plate increases the surface of the model along the divergent boundary, and lengthens the transform boundary (Fig. 1c). As a consequence, the amount of finite displacement varies along the transform boundary. It is constant and equal to the plate displacement along most of the transform boundary, but decreases to zero towards the intersection with the divergent boundary (Fig. 1c). This is similar to the displacement pattern expected to occur at a transform margin during the syn-rift stage (Basile et al., 1993) or inside an oceanic rift at a ridge–transform intersection.

The model consists of a lower ductile layer (silicone putty), and an upper brittle layer (sand). It is constructed so as to be analogous to the ductile–brittle layering of continental crust (Allemand and Brun, 1991; Davy and Cobbold, 1991). In the upper sand layer, faulting occurs according to the Mohr–Coulomb criterion (Hubbert, 1951; Mandl et al., 1977) with a coefficient of friction (ϕ = tan 30°–32°) similar to the so-called Byerlee law (Byerlee, 1978). In the lower silicone layer (Rhône-Poulenc GS1R gum), deformation follows a Newtonian law, with a viscosity of 2×10^4 Pas at room temperature (Nalpas and Brun, 1993, appendix 1). The strength of the silicone layer depends on the product of viscosity and strain rate, the latter being controlled by the velocity of the mobile basal plate. In the present experiments, scaling of boundary displacement rates allows simulation of the deformation of the lower ductile crust (Davy and Cobbold, 1991). The basal plate on which the silicone layer lies is designed to simulate the top of the lithospheric mantle. Therefore, displacements applied at the base of sand–silicone models allow the study of crustal-scale effects associated with a lithospheric plate boundary. However, in our experiments, the rigidity of basal plates prevents vertical displacements and corresponding isostatic effects.

The brittle layer is made of alternate layers of coloured sand, used as passive horizontal markers. A square grid of coloured sand is traced on the surface of each model. During deformation, time-lapse photographs record the distortion of the upper grid. At the end of the experiment, the sand is wetted and vertical sections are cut in the deformed model to study internal deformation.

Table 1
Parameters used in the performed experiments

Experiment PA: pull-apart TM: transform margin	Length of divergent boundary (cm)	Lengths of transform boundaries (cm)	Sand thickness (cm)	Silicone thickness (cm)	Sand/silicone thickness ratio	Bulk velocity (cm/h)	Total displacement (cm)	Basin infilling
PA1	14.5	31.5–26.5	3	1.5	2	1	5	–
PA2	14.5	31.5–26.5	3	1.5	2	2	8	+
PA3	14.5	31.5–26.5	3	1.5	2	10	15	+
PA4	14.5	31.5–46.5	2	1	2	1	8	+
PA5	17	34–34	2	1	2	2	12	+
PA6	9	39–39	2	1	2	2	13	+
PA7	17	39–39	2	1	2	1	12	+
PA8	20	44–44	2	1	2	2	13.5	+
TM1	36	43	3	1	3	15	20	+
TM2	36	43	3	1	3	5	20	+
TM3	36	43	3	1	3	5	20	–
TM4	32.5	40	2	1	2	10	25	–
TM5	45	40	2	1	2	10	25	–
TM6	45	50	2	1	2	10	25	–
TM7	45	40	2	1	2	10	25	–
TM8	45	40	2	1	2	10	12	–
TM9	29.5	40	4	0	—	10	15	–

Seventeen experiments were performed with different experimental parameters (varying the sand and silicone thicknesses, bulk velocity, total displacement, sizes of the Riedel box, basin infilling) (Table 1). Only two examples of each type of experiment (Fig. 1) are described in detail. The results of other experiments are summarized. Since the study is focused on the interaction between transform and divergent components of deformation, we do not present the deformational patterns observed above pure transforms (Emmons, 1969; Tchalenko, 1970; Naylor et al., 1986; Basile, 1990; Mauduit and Dauteuil, 1996) or divergent boundaries (Allemand et al., 1989; Allemand and Brun, 1991; Tron and Brun, 1991).

3. Pull-apart type experiment

3.1. Experiment PA5

Deformation starts as a simple shear in a wide elongated area joining the two transform boundaries. Strike-slip faults appear first at the edges of transform boundaries and propagate towards the centre of the model (Fig. 2a and b). They can be compared with synthetic Riedel (R) faults, but their obliquity with the transform boundary is greater (30°) than the angle of 15° expected from the Mohr–Coulomb theory or from similar experiments made only with sand (Faugère et al., 1986; Horsfield and Naylor, cited by Mandl, 1988). This unexpected strike of the R faults is a primary consequence of the interaction between transform and divergent motions in a ductile–brittle model. As the basal ductile layer (silicone) allows the stresses to propagate laterally, stresses are of pure strike-slip type at the extremities of the transform boundaries, and show strike-slip and extensional components in the rest of the model. By reference to a true dextral Riedel shear experiment, the trend of R type faults is rotated clockwise by the extensional component.

With increasing displacement, R faults become rapidly inactive, and the strike-slip movement is accommodated by new faults parallel to the basal transform boundary (Y faults according to Bartlett et al., 1981). Progressively, Y faults connect with R faults, and a sigmoidal strike-slip fault set cuts across the whole model (Figs. 2c, d, 3a and b). The sigmoidal fault set which does not follow the plate boundaries, trends oblique to the releasing stepover. It is noteworthy that, in experiments only using brittle materials (Faugère et al., 1986; Hempton and Neher, 1986; Horsfield and Naylor, cited by Mandl, 1988; McClay and Dooley, 1995), the sigmoidal fault set is located directly above the basal boundaries.

New faults appear above the divergent plate boundary (Figs. 2c and 3a). Considering their trends (65°) and slight left-lateral displacements, they can be compared to antithetic Riedel (R′) faults. As for the previous R-type faults, strike-slip displacement along these faults remains limited.

At the end of the experiment, strike-slip displacement is accommodated exclusively by Y faults above the basal transform boundaries (Figs. 2e and 3c). Most of the previous faults are active, and accommodate transtension. For example, the early R type faults display vertical offsets which indicate later activation as

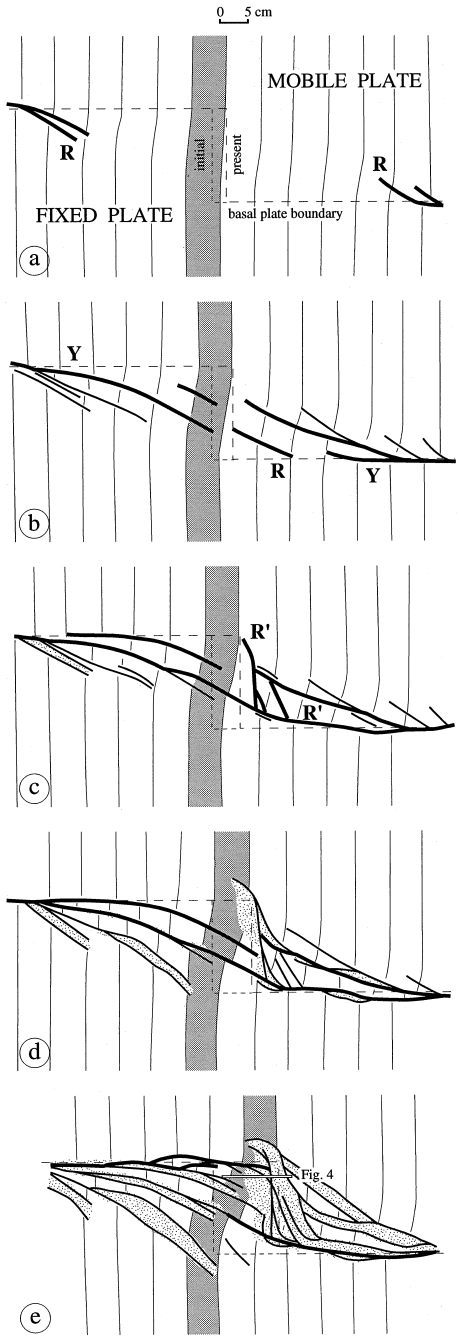

Fig. 2. Surface views during experiment PA5. Bulk displacements 1.5, 3, 4, 6 and 12 cm for (a), (b), (c), (d) and (e), respectively. For photographs of (c–e), see Fig. 3. Stippled lines indicate the position of the basal plate boundary at each stage, and its initial position. Thin lines and shaded bands are passive markers placed at the surface of the model. Thick lines indicate faults; the thickest lines indicate active strike-slip faults. Dots show basins infilled by sand during the experiment. In (e) the bar shows location of the section in Fig. 4.

oblique slip. At this final stage, the active fault set is similar to the one expected for a pull-apart basin (Figs. 2e and 3c): two dextral strike-slip fault sets define a right-lateral stepover. Within the stepover area, an asymmetric basin is formed, bounded on one side by a R′ listric fault. The progressive deepening of the basin on the other side corresponds to a roll-over bending of the sand layer (Fig. 4). Transtension on R′ faults is directly connected to the basal divergent boundary located immediately beneath.

It is interesting to note the progressive evolution of the R′ fault from Fig. 2(c) to (e) (see also Fig. 3a–c). This fault terminates with a strong curvature toward the junction with the transform basal boundary. This results from the strong gradient of thinning and consequent gravity potential which occurs across the transform boundary. On the basin side, thinning is strong allowing a component of gravitational gliding on the opposite side of the transform boundary. This illustrates the local role of body forces in the development of pull-apart basins, an effect that is further illustrated in the transform margin experiment described in the next section.

While bulk surface displacements are roughly parallel to the basal boundary displacement, clockwise block rotations around the vertical axis also occur in the brittle layer. Rotations mainly result from internal deformation due to strike-slip shearing prior to faulting (Fig. 2). The amount of rotation remains low where the model is not thinned (early faulting), but can reach values as high as 20° in thinned areas (late faulting) (Fig. 5) (Cobbold et al., 1989; Jolivet et al., 1991).

3.2. Other pull-apart experiments

The other pull-apart type experiments carried out in this study (Fig. 6) show sets of faults that can differ from the experiment PA5 described above (Fig. 2). In some of them (PA4, PA6 and PA8), significant corner effects develop due to silicone flow at the edges of the model. More important are the variations of the acute angle between R faults and the direction of basal transform boundaries. The mean angle is 30°, as in experiment PA5 (Fig. 2), but can fall to 22° when the bulk displacement rate increases (experiment PA3, Fig. 6) or when the length of the divergent boundary is reduced (experiment PA6, Fig. 6).

The angles between R′ faults and bulk displacement remain approximately constant in all experiments, but R′ faults do not always develop in the same way. When the bulk displacement rate increases, leading to an increase of the ductile layer strength, R′ faults become more numerous. They are located between R faults (experiment PA3, Fig. 6), and are not only restricted to the vicinity of the divergent plate boundary as in experiments PA5 (Fig. 2), PA4 and PA8 (Fig. 6).

Finally, the timing of R′ fault development appears to control the shape of the basin. Pull-apart basins

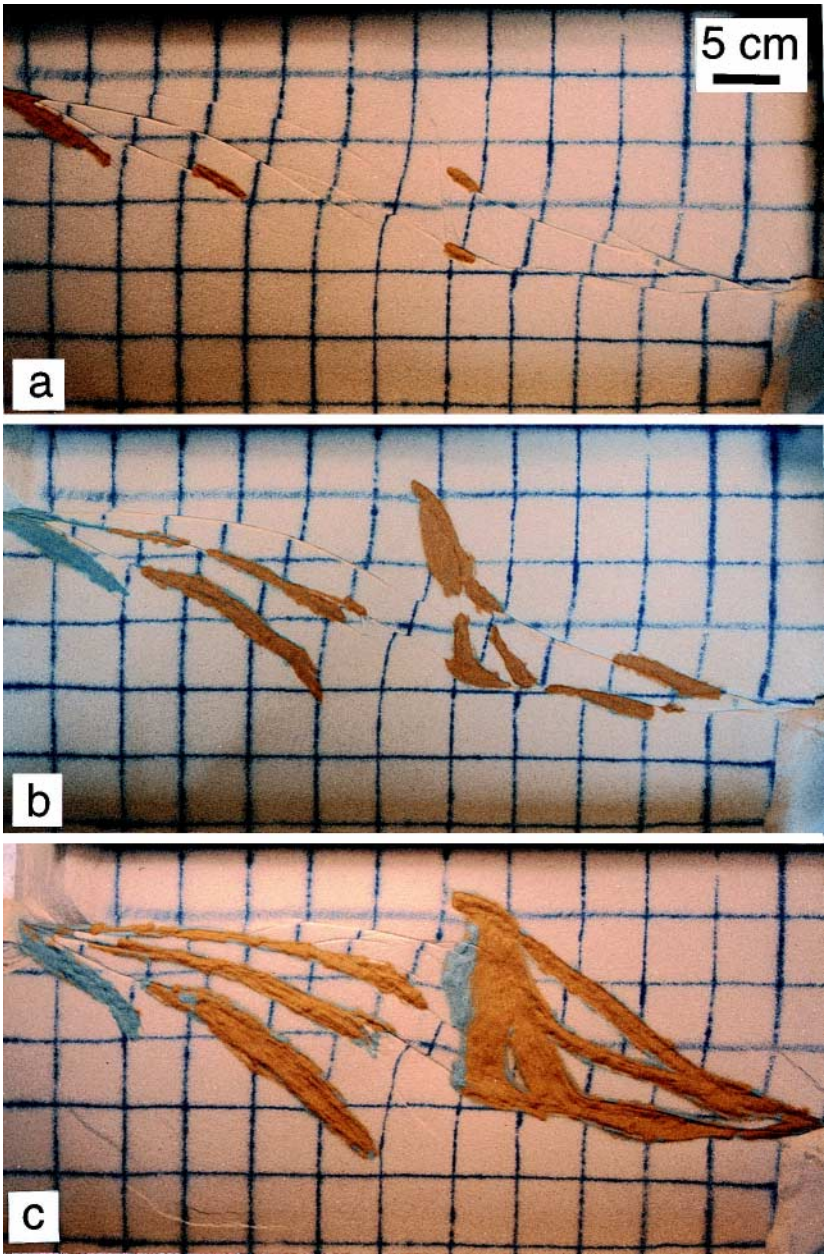

Fig. 3. Surface views during experiment PA5. Bulk displacements 4, 6, and 12 cm for (a), (b) and (c), respectively. For line drawings see Fig. 2(c–e).

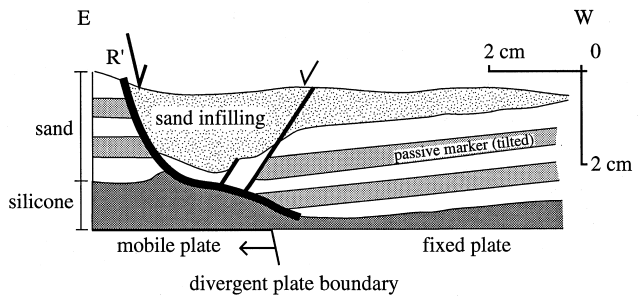

Fig. 4. Section of the asymmetric basin in experiment PA5. Location Fig. 2(e).

remain elongated and sigmoidal before R′ faults appear (PA1, PA2, PA6 and PA7), or become rhomb-shaped along with the development of R′ faults. In PA3, PA4, PA5 and PA8 experiments, the two successive stages are superimposed.

4. Transform margin type experiment (TM5)

Pull-apart experiments allow the study of the modes of connection between two stepover transform faults, while transform margin experiments focus on defor-

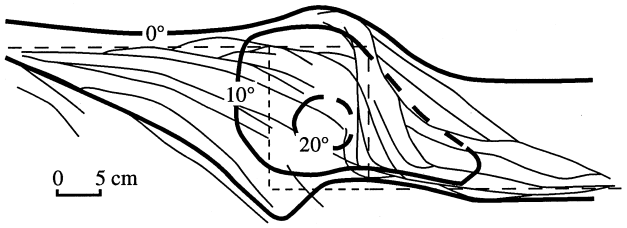

Fig. 5. Magnitude of clockwise rotation at the end of experiment PA5 (modified from Cobbold et al., 1989). Contours in degrees. The fault set from Fig. 2(e) is superimposed.

mation at the intersection of divergent and transform plate boundaries.

In this experiment, normal faults develop prior to strike-slip faults, as expected from the reduced strength in extensional regime compared with the shear regime. A rift develops directly above the divergent plate boundary (Figs. 7 and 8) (for structure and formation of rifts in brittle–ductile systems, see Allemand and Brun, 1991). As in pull-apart experiments, a zone of simple shear is observed above the transform plate boundary. En échelon R faults then successively develop from the model edge (fault 1) towards the centre of the model (faults 2–6, Fig. 7a). At the intersection between transform and divergent plate boundaries, normal faults develop with an en échelon pattern (Figs. 7a and 8a), and curved strike-slip R faults connect up with the normal faults (faults 4 and 5, Figs. 7a, b, 8a and b).

As displacement increases, R faults located above the transform boundary become connected to Y faults to form a Principal Displacement Zone (PDZ, Tchalenko and Ambraseys, 1970). The PDZ is a narrow trough, parallel to displacement, which is cut by anastomosed faults (Figs. 7c, d, 8c and d). Towards the divergent boundary, the PDZ widens out into a horsetail splay of curved strike-slip faults (faults 5–7 in Figs. 7b and 8b). The horsetail splay lengthens progressively as new curved strike-slip faults develop near the divergent boundary (faults 8 and 9 in Fig. 7c; faults 10–13 in Figs. 7d, 8c and d). Blocks bounded by these faults rotate clockwise up to 25° during faulting and are displaced towards the extensional basin. Older curved strike-slip faults that have become inactive are then passively rotated, displaced and cut by new faults. This is exemplified by the rotation and displacement of fault 7 (from Fig. 7b to 7d), which is finally cut by the PDZ (Figs. 7d and 8d).

Serial sections across the horsetail splay illustrate the gradient of thinning that occurs across the transform boundary (Fig. 9). The corresponding surface slope shows a trend perpendicular to the slope of the extensional basin. The thinning of the brittle layer in the horsetail splay is accommodated by tilting of the blocks separated by the curved strike-slip faults which are later rotated around a vertical axis and displaced toward the basin. Note that these faults, which are related at depth to the basal transform boundary, dip opposite to the surface slope.

Similarly, deformation evolves in a relatively complex way at the junction of the horsetail splay with the extensional basin. Cross-sections show the occurrence, within the basin, of an overturned anticline associated with reverse faults (Fig. 9a and b). These reverse faults initiate as normal faults above the divergent boundary (shaded faults in Fig. 7c and d). Due to dextral shearing along the horsetail splay, they rotate clockwise up to 80° (Fig. 7c and d) and give rise to a local positive inversion. This peculiar and rather unexpected deformation occurs when the thinning becomes intense within the basin. When this occurs, most of the transform motion between the two basal plates migrates from the transform boundary to the thinner and weaker part of the model.

5. Discussion

5.1. Geometry of experimental pull-apart basins

During the first stages of a pull-apart experiment in a ductile–brittle model, faulting occurs only by R faults above transform boundaries. A pull-apart basin geometry appears only when transform boundaries connect up with each other (Fig. 10). Connecting segments are parallel to R faults and make a mean angle of 30° with the transform boundary. Y faults develop simultaneously above the transform boundaries. The combination of active strike-slip R and Y faults defines elongated pull-apart basins (PA5, Fig. 2b and c; PA7, Fig. 6), comparable to the 'lazy Z-shaped' basins (S-shaped for a left lateral strike-slip) of Mann et al. (1983), and to many natural examples (e.g. Timna graben: Freund et al., 1968; Dasht-e Bayaz: Tchalenko and Ambraseys, 1970; Hanmer Plain: Freund, 1974; Cantil Valley: Aydin and Nur, 1985). At the end of this early stage, extension takes place along and between R faults.

The experiments demonstrate that this type of pull-apart basin geometry develops in brittle–ductile systems at rather small strike-slip displacement. Similarly, field studies indicate that similar natural examples, especially small pull-apart basins (from 0.5 to 13 km in length), probably correspond to limited amounts of strike-slip displacement. As an example, the length of the Hanmer Plain pull-apart basin is 13 km, while the horizontal slip along the fault is 20 km (Freund, 1974). Moreover, theoretical considerations of elastic interaction between two stepover strike-slip faults lead to a similar geometry by lengthening of faults and their

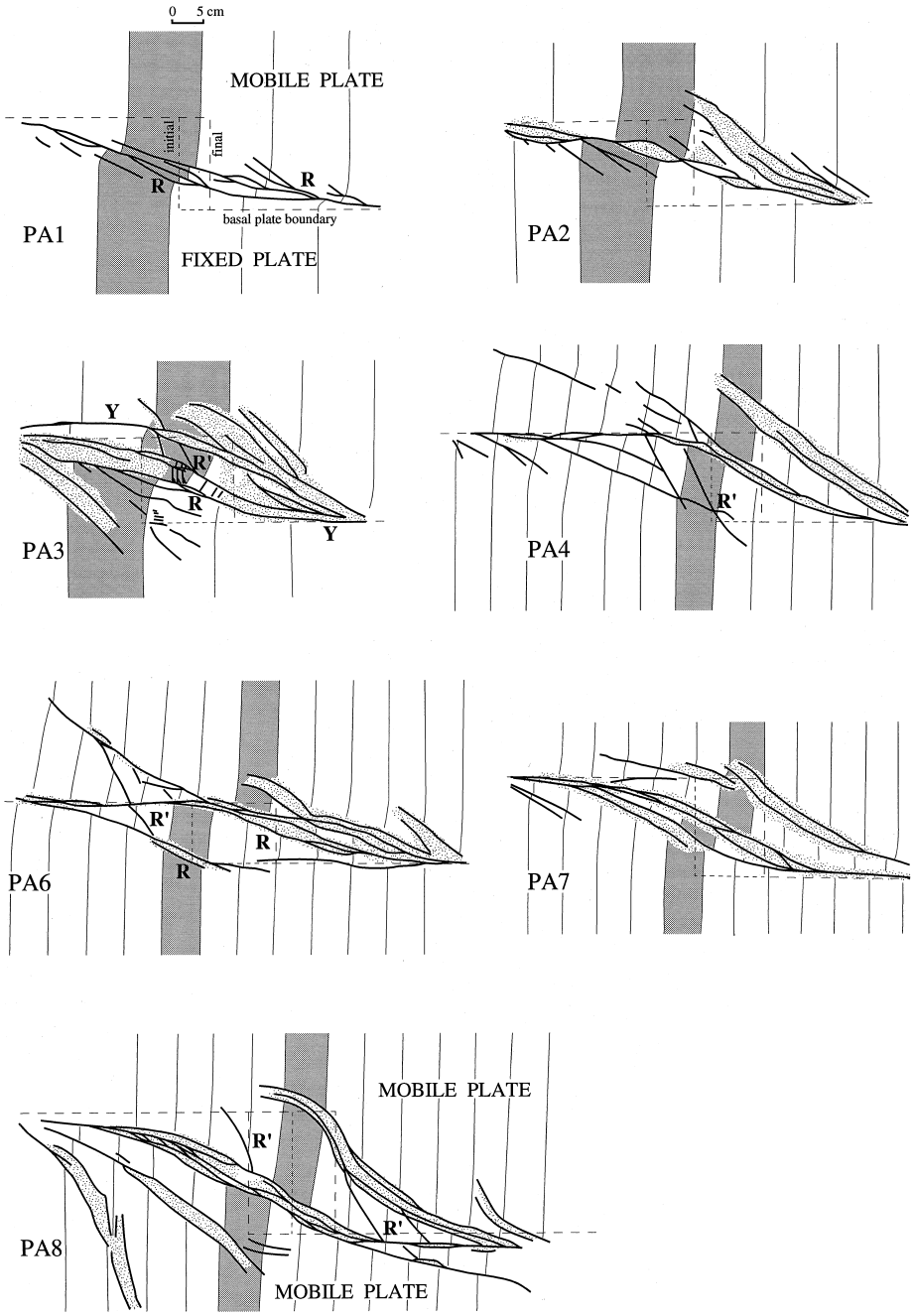

Fig. 6. Surface views at the end of PA experiments. Same scale in all experiments, and same legend as in Fig. 2. PA8 is the only experiment carried out with a symmetrical apparatus. The left-lateral displacement on R′ faults can be seen in experiments PA4, PA6 and PA8.

connection by oblique faults (Rodgers, 1980; Segall and Pollard, 1980).

Later on in the experiments, R′ faults start developing near the divergent boundary (PA4 and PA8, Fig. 6; PA5, Fig. 2c–e), and delimit a new border for the basin. This is observed in natural rhomb-shaped grabens [e.g. Bir Zreir: Eyal et al., 1986 (Fig. 11); Mesquite Lake: Johnson and Hadley, 1976; Coyote Creek fault: Bahat, 1982; or Barahta graben: Heimann et al., 1990]. In experiment PA8 (Fig. 6), the two basal plates are mobile, and extension is symmetric on both sides of the basin. Consequently, R′ faults appear on both sides of the basin, giving a basin geometry similar to the classical shape of a pull-apart basin (e.g. Gulf of Elat: Ben-Avraham, 1985) (Fig. 12). In asymmetric experiments, extension takes place mainly on the R′

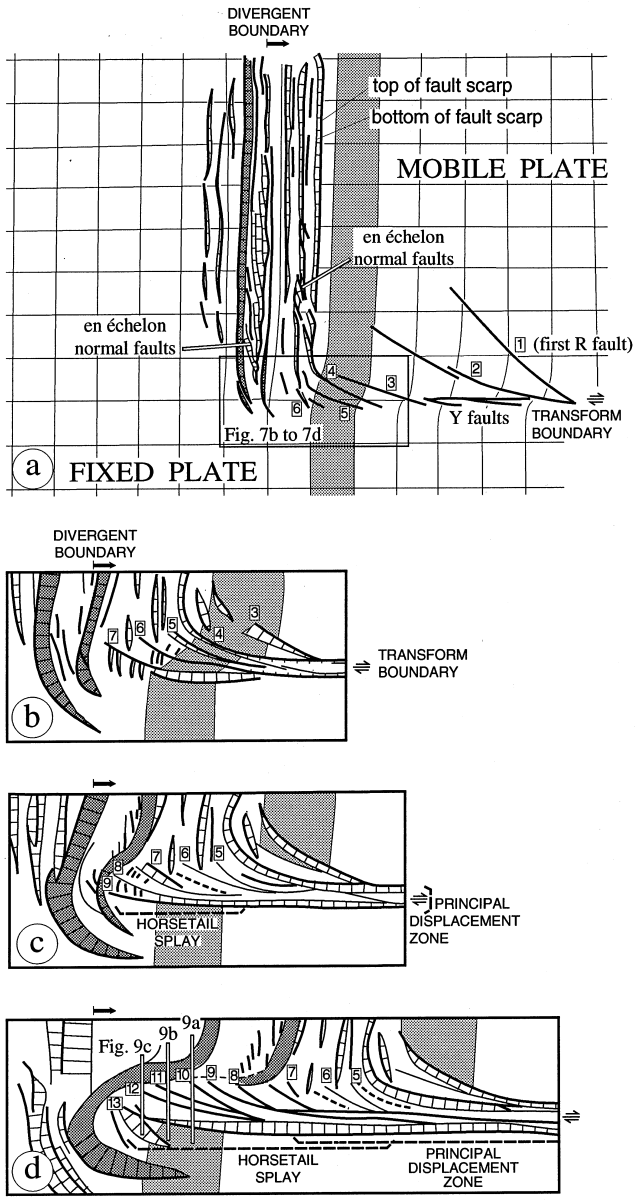

Fig. 7. Surface views during experiment TM5. Bulk displacements 4, 8, 12 and 25 cm for (a), (b), (c) and (d), respectively. (b–d) are enlarged from the box shown in (a). Narrow lines are passive markers (spacing 5 cm), and thick lines are faults. Passive markers (light grey) and two normal faults (dark grey) are underlined to illustrate the offset by the transform zone. Numbers (1–13) indicate the order of appearance of R faults. In (d) bars locate the sections shown in Fig. 9.

fault hanging wall, resulting in tilting and/or roll-over bending which define asymmetric basins. This is also seen in many natural pull-apart basins (e.g. Dead Sea basin: Zak and Freund, 1981; Manspeizer, 1985; Kashai and Croker, 1987; Kineret Lake: Ben-Avraham and Ten Brink, 1989; Salt Lake basin: Zhang et al., 1989).

5.2. Scale independence of pull-apart basins

From a compilation of the dimensions of 62 active pull-apart basins, Aydin and Nur (1982) found a relationship between the length (l) and width (w) of a pull-apart basin:

$$\log l = c_1 \log w + \log c_2, \quad (1)$$

with $c_1 \approx 1$ and $2.4 < c_2 < 4.3$, with a mean value of 3.2 (Fig. 13). So

$$2.4 < l/w < 4.3. \quad (2)$$

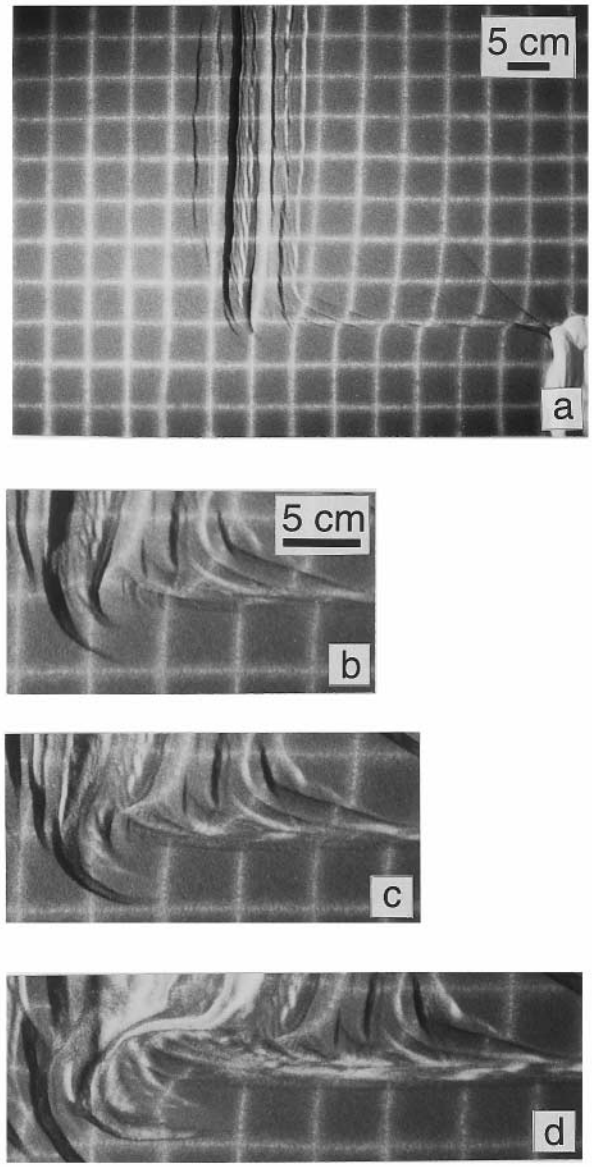

Fig. 8. Surface views during experiment TM5. Bulk displacements 4, 8, 12 and 25 cm for (a), (b), (c) and (d), respectively. (b–d) show details from the rift-transform intersection. For line drawings see Fig. 7(a–d).

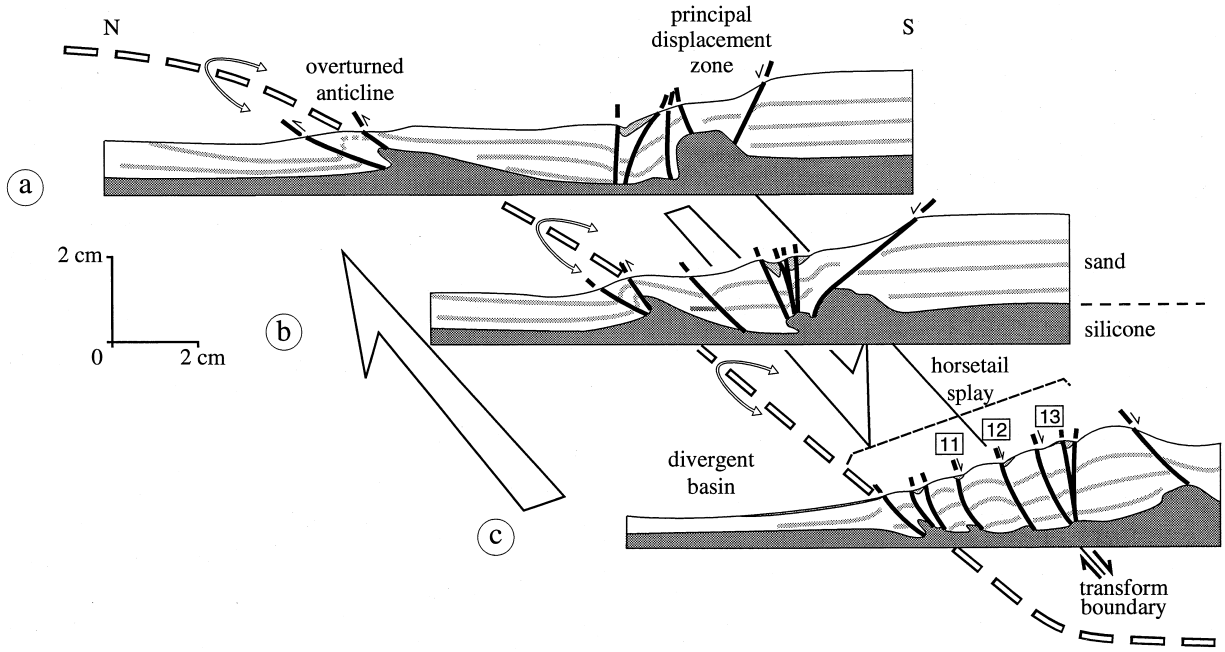

Fig. 9. Sections of the transform zone along the divergent basin in experiment TM5. Location shown in Fig. 7(d).

In experiments, the geometry of the basal plate boundary imposes the width w of the basin, and the plate displacement imposes a l/w ratio of around 1 at the base of the model (Table 2 and Fig. 13). As described above, the first basin that appears is bounded by connected R and Y faults (Fig. 10). Assuming that Y faults are parallel to the bulk displacements, the l/w ratio depends on angles α and β (acute angles between Y and the two R faults, Fig. 10):

$$l_s/w_s = 1/\tan\alpha + 1/\tan\beta, \tag{3.1}$$

or

$$l_m/w_m = 1/\sin\phi\cos\phi, \tag{3.2}$$

where l_s is measured parallel to the bulk displacement, l_m is the longest diagonal of the basin, w_s and w_m are basin width measured perpendicular to l_s and l_m, respectively, and where $\tan\phi = (\tan\alpha\ \tan\beta)/(\tan\alpha + \tan\beta)$ (Fig. 10). Ratios l_s/w_s and l_m/w_m are both given here because Aydin and Nur (1982) do not indicate which ratio was used in their study.

From the experiments, the mean angle between R and Y faults is $\alpha = \beta = 30°$. An ideal basin of this type, bounded by R and Y faults (Fig. 10), is therefore characterized by $l_s/w_s = 2/\tan30° = 3.5$ and $l_m/w_m = 3.8$. The l/w ratios obtained from Eq. (3.1) and (3.2) are close to the ratios observed in experiments at small displacement of basal plates (Fig. 10), but are inconsistent with the ratios imposed by geometry and displacement of basal plates (Table 2 and Fig. 13). For example, in experiments PA7 and PA6, l_m/w_m ratios are 3.8 and 4.6, respectively, while the ratios applied at the model base are only 1.44 and 0.71, respectively. In other words, the length of a pull-apart basin in experiments does not depend on the horizontal slip of the bounding strike-slip faults.

When displacement increases, the pull-apart basin becomes limited by Y faults above the transform boundaries, and also by R and R′ faults on the other sides. As the R′ faults make an average angle of 65° with the Y faults, the resulting basin is characterized by $l_s/w_s = 1/\tan30° + 1/\tan65° = 2.2$ and $l_m/w_m = 2.6$.

Consequently, for the early stages of pull-apart basin development, Eq. (3.1) and (3.2) give $2.2 < l/w < 3.8$, which is consistent with $2.4 < l/w < 4.3$ found by Aydin and Nur (1982) (Fig. 13). Our experiments suggest that the 'scale independence' advocated by Aydin and Nur (1982) can simply result from the bordering fault patterns (association of R or R′ and Y faults with characteristic angles of obliquity) that develop above a deeper stepover between two strike-slip faults, instead from coalescence of elementary pull-apart basins (see fig. 6 in Aydin and Nur, 1982).

At each stage, acute angles between Y and R or R′ faults can vary in experiments (for example PA3 and PA6, see above) as in field examples (Bahat, 1983). These angles depend on initial conditions: bulk displacement rate, width of the divergent plate boundary (Table 1) and the angle between transform and divergent boundaries (Jolivet et al., 1991; Dooley and McClay, 1997). In experiments, the angles between Y and R′ faults are nearly constant (from 55 to 65°), but R′ faults can connect to other faults through segments at lower angles. The angles between Y and R faults

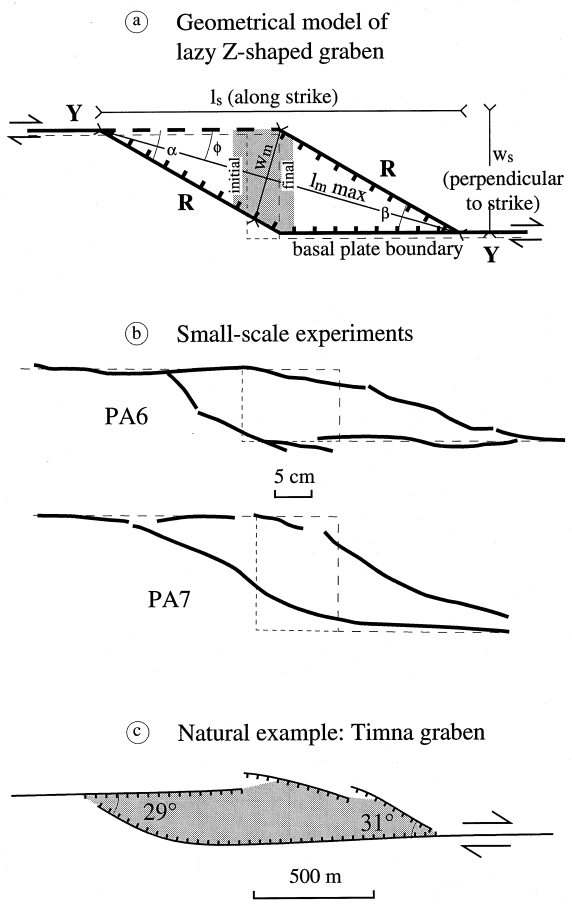

Fig. 10. Initial shape of a pull-apart basin: lazy Z-shaped basin. (a) Geometrical model, where only active faults are shown. Stippled faults do not occur in all experiments. Shaded area indicates subsiding basins. (b) Experimental examples (end of experiments PA6 and PA7). Thick lines are faults. (c) Natural example from the Dead Sea transform: the Timna graben (modified from Freund et al., 1968). Shaded area indicates subsiding basins. Strike-slip faults are sinistral in this example, but the map has been inverted to make them dextral as in the experiments.

may also be less than 30°. Natural examples of pull-apart basins compiled by Bahat (1983) show a mean acute angle of 35° (Fig. 14). In such examples, only a few basins have angles between bounding faults that are higher than 60°. In natural examples of pull-apart basins as well as in experiments, angles between bounding faults can be less than 30° (R faults) or 65° (R′ faults), but are rarely more. As the $2.2 < l/w < 3.8$ ratio is computed from Eq. (3.1) and (3.2) using two R faults for the upper limit and an R and an R′ fault for the lower limit, this ratio can only increase when acute angles between faults decrease.

Moreover, because the basin length increases with plate displacement, while the width remains constant, Eqs. (3.1) and (3.2) are expected to yield minimal values. In experiments, the final displacements are large [e.g. 12 cm in experiment MT5 (4 times the total thickness of the model), corresponding to 120 km of strike-slip displacement in a 30-km-thick crust]. Even for large displacements, l/w is rarely higher than 3 in experiments because R′ faults replace R faults in delimiting the basin border. The resulting change in basin shape reduces the length and l/w ratio.

In nature, only a few large pull-apart basins have l/w ratios higher than 5. Mann et al. (1983) have suggested that the constant l/w ratio of active basins may reflect the tendency of older basins with higher ratios to be hidden by sedimentation and the displacement of active strike-slip faults. The Dead Sea Basin is one of these very elongated basins, with a length of 130 km and a width of 18 km ($l/w = 7.2$) (Zak and Freund, 1981). In fact, the Dead Sea Basin is formed by the coalescence of three successive and adjacent

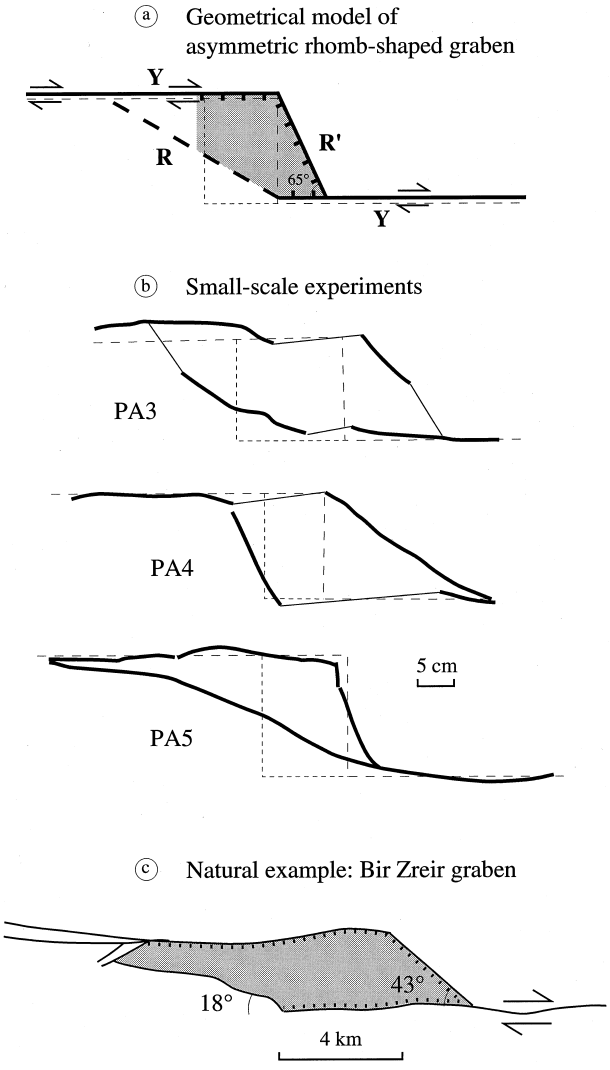

Fig. 11. Rhomb-shaped graben stage in an asymmetrical setting. Same legend as Fig. 10. (a) Geometrical model. (b) Experimental examples (end of experiments PA3, PA4 and PA5). Thin lines are interpolations between faults made to close the basins. (c) Natural example from the Dead Sea transform: the Bir Zreir Graben [modified (inverted map) from Eyal et al., 1986].

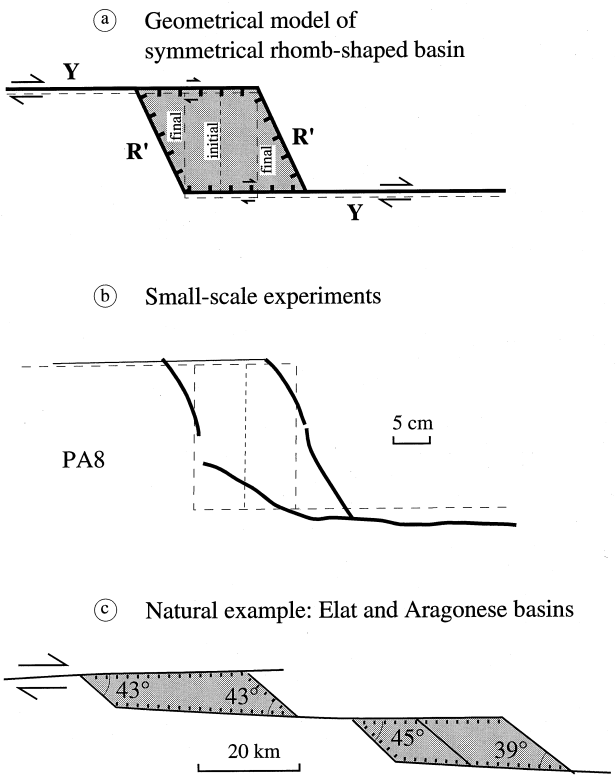

Fig. 12. Rhomb-shaped graben stage in a symmetrical setting. Same legend as Fig. 10. (a) Geometrical model. (b) Experimental example (end of experiments PA38). Thin line is interpolation between faults made to close the basin. (c) Natural example from the Dead Sea transform: the Elat and Aragonese basins [modified (inverted map) from Ben-Avraham, 1985].

sedimentary basins whose depocentres have migrated northward with time (Zak and Freund, 1981). Each sub-basin has an l/w ratio (2.4, 3.3 and 2.6 from south to north) that is consistent with Eq. (2) (Fig. 13).

This suggests that a single pull-apart basin cannot exceed an upper limit for l/w. The explanation proposed by Aydin and Nur (1982) considers the coalescence of rhomb grabens associated with pre-existing strike-slip faults. Following Mann et al. (1983), and on the basis of experiment analysis, we consider that changes in location and activity of master strike-slip faults provide a better explanation. Thus, the l/w ratio limit and depocentre migration may result from a horizontal migration of the stepover which can occur when the crust becomes thin enough within the pull-apart basin. Stepover migration cannot be achieved in the present experiments since the stepover location is imposed by basal plate boundaries. In nature, stepover horizontal migration probably occurs by propagation of one of the transform faults through the whole lithosphere and step-by-step inactivation at the tip of the other (Fig. 15).

5.3. Rift-transform intersection and horsetail splay

In oceanic basins, marginal ridges are common features of transform margins (e.g. South Newfoundland: Grant, 1977; Liberia and Ivory Coast–Ghana: Delteil et al., 1974; South Agulhas: Scrutton, 1976). They appear as elongated highs at the continental border, striking parallel to the transform margin and the adjacent oceanic fracture zone. In cross-section, they are always located between an extensional basin (divergent margin or intracontinental basin) and the oceanic crust. These marginal ridges are not of magmatic origin, being commonly composed of continental rocks (basement and/or sediments). Several hypotheses have been proposed to explain the development of marginal ridges at transform margins, either by tectonic, thermal or magmatic underplating mechanisms (review by Basile et al., 1993).

Otherwise, marginal ridges appear at transform-divergent intersections, i.e. in the same kinematic setting as the horsetail splay in TM experiments (Fig. 7). Many similarities have been found between experiments and typical marginal ridges such as the Ivory Coast–Ghana ridge (Basile et al., 1993). The northern slope of the marginal ridge, as well as the slope of the horsetail splay, is perpendicular to the slope of the adjacent divergent basin. En échelon strike-slip faults are arranged along the slope. In Ivory Coast–Ghana,

Table 2
Lengths and widths of pull-apart basins in PA experiments. Experiments PA1 and PA2 did not reach a pull-apart stage

Experiments	Bounding faults	l_s (cm)	w_s (cm)	l_m (cm)	w_m (cm)	l_s/w_s (base)	l_s/w_s (surface)	l_m/w_m (surface)
PA3	YR′YR	40.5	13.3	43.4	14.3	1.03	3	3
PA4	YR—R′	35.5	15.3	37.8	16.3	0.55	2.3	2.3
PA5	YR′YR	26.8	13.7	29.6	10	0.67	2	3
PA6	YRYR	40.8	10	41.7	8.9	0.71	4.1	4.7
PA7	YRYR	39.4	15.1	41.7	11	1.44	2.6	3.8
PA8	—R′YR′	26	22	34	15.9	0.71	1.2	2.1

l_s is the along-strike length, l_m is the maximal length (Fig. 10), w_s and w_m are perpendicular to l_s and l_m, respectively. Measurements were performed with the set of faults shown in Figs. 10–12. l_s/w_s (base) is the displacement imposed at the base of the model vs the length of the divergent plate boundary (i.e. width of the basin)

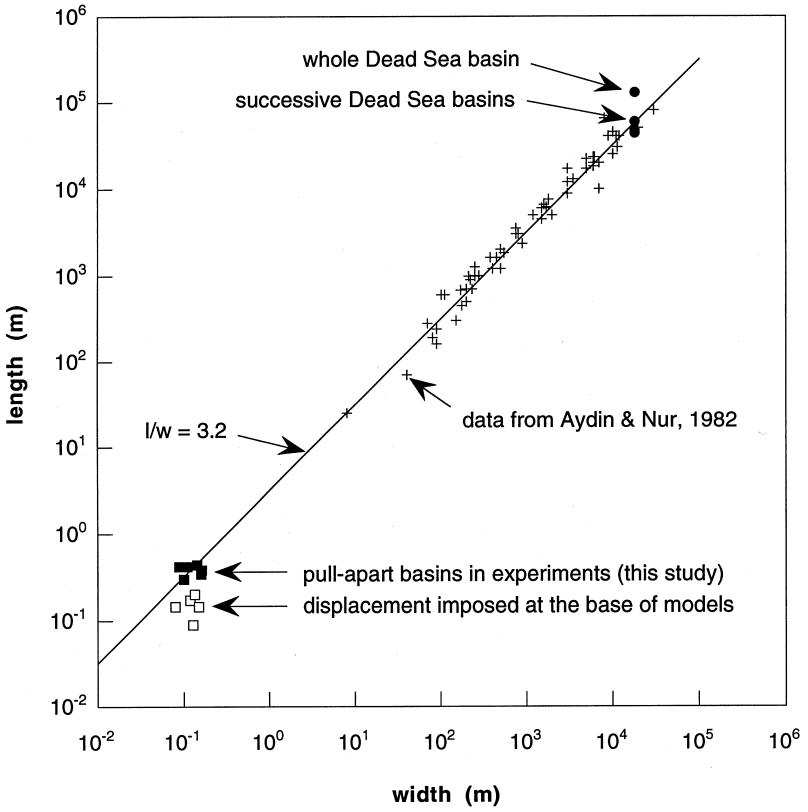

Fig. 13. Log length vs log width plot for natural pull-apart basins (data from Aydin and Nur, 1982) and experiments. The straight line shows the relation $l/w = 3.2$ defined by Aydin and Nur, 1982. Filled dots indicate location of Dead Sea basins (from top to bottom: whole basin, Sedom, Dead Sea and Hazeva, cf. Fig. 15). Open squares indicate displacement (length) vs width of the stepover imposed at the base of experiments PA3 to PA8 (PA1 and PA2 are not given because they did not reach a pull-apart stage); filled squares indicate l_m and w_m measured at the end of experiments PA3 to PA8.

terminations of such faults show dip-slip and ridge tilting that are contemporaneous with the rifting of the adjacent divergent basin. In experiments, the dip-slip displacements and block tilting are also contemporaneous with rifting. Because of the kinematic setting, the horsetail splay progressively propagates towards the transform-divergent intersection. Consequently, the faults are younger towards this intersection, and, in

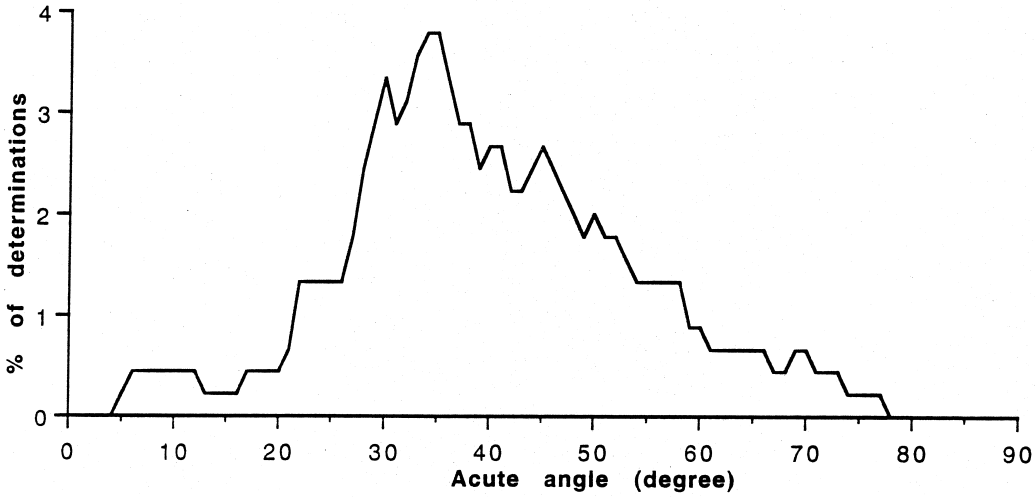

Fig. 14. Frequency histogram for acute angles between border faults in natural pull-apart basins (data from Bahat, 1983). Only data from shear-related basins are included. The histogram is smoothed at 9° (measurement accuracy is ±5°).

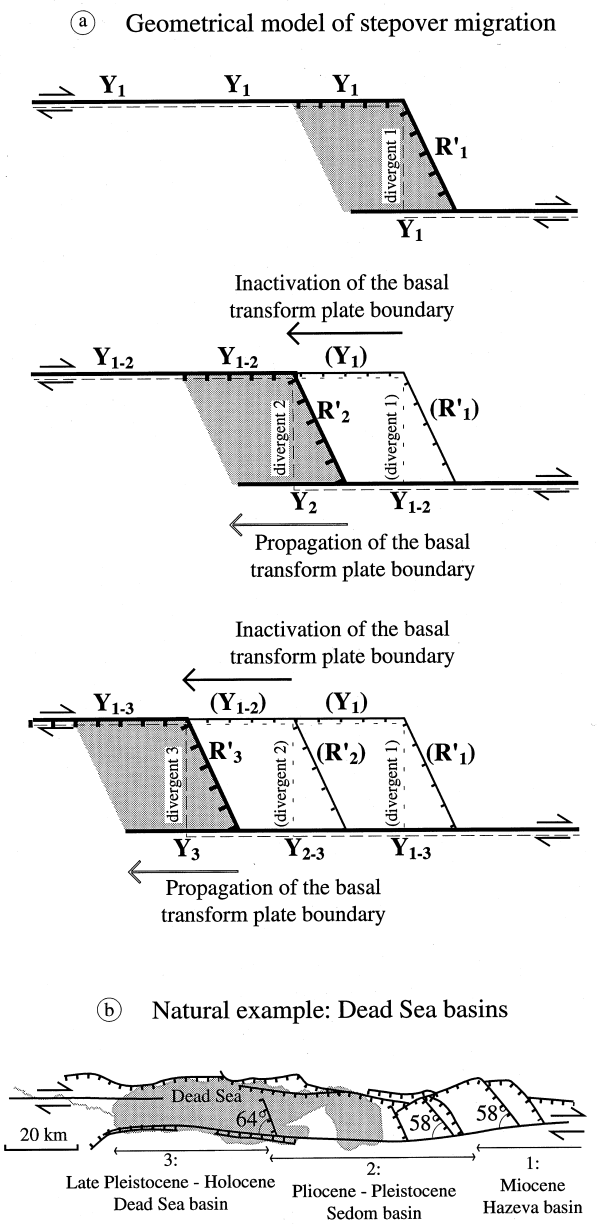

Fig. 15. Stepover migration and coalescence of rhomb-shaped grabens. Same legend as Fig. 10. (a) Geometrical model of stepover migration from a single rhomb-shaped basin (Figs 11 & 12). Three successive stages are shown. Thick lines indicate active faults, thin lines are inactive faults. Subscripts in Y_1, Y_{1-2}, etc., indicate the time of strike slip faulting on each segment. (b) Natural example from the Dead Sea transform: the Dead Sea basins [modified (inverted map) from Zak and Freund, 1981 and Kashai and Croker, 1987]. Stepover migration cannot occur in experiments because of the rigidity of the basal plates.

the opposite direction, the older faults are cut by the active PDZ. Similar features and kinematic development have been revealed by seismic data in the Ivory Coast–Ghana marginal ridge (Basile et al., 1993), where strike-slip deformation decreases towards the transform-divergent intersection, while the top of the ridge is highly deformed by numerous wrench faults.

We propose that en échelon strike-slip faults occurring along the northern slope of the Ivory Coast–Ghana marginal ridge belongs to a horsetail splay that is contemporaneous with the rifting in the adjacent divergent basin. Marginal ridges of transform margins develop at least partly during the divergent rifting by block tilting in the horsetail termination of a strike-slip fault.

6. Conclusions

This study presents experiments aimed at understanding the deformation of a ductile–brittle model above a releasing step of deeper strike-slip faults. The experiments give new insights into the development of pull-apart basins and transform margins:

1. Crustal scale faulting and the resulting fault pattern strongly depend on the rheological layering. The location of strike-slip faults in the experiments, as well as the number and strike of faults vary with the presence of a ductile layer at depth. In purely brittle models, the fault set at the surface reproduces the shape of imposed basal discontinuities. In ductile–brittle models, strike-slip faults propagate from the transform boundaries, and then connect up to form the sigmoidal shape of pull-apart basins. The shape of the pull-apart basin together with the number, orientation and location of strike-slip and normal faults are controlled by the strength of the ductile layer and the width of the basal stepover.
2. Successive stages with distinct basin shapes can occur during the development of pull-apart basins. In experiments, successive stages of this evolution can be observed, whereas only the final stage is observed in nature. The first stage corresponds to a lazy S- or Z-shaped basin (for respectively left- and right-lateral motion) made by connection of R faults propagating from each side of the stepover with Y faults directly above the transform boundaries. A second stage is rhomb-shaped graben, bounded on one or both sides by R′ faults accommodating extension. The symmetry or asymmetry of the pull-apart basin occurring along strike depends on the symmetry or asymmetry of the basal divergent boundary. This final stage may evolve during displacement by propagation of one of the master strike-slip faults and inactivation of the other. This induces displacement of the stepover, and subsidence in a newly created pull-apart basin.
3. ‘Scale independence’ of pull-apart basins follows the same law in nature as in the experiments.

Approximately constant length vs width ratio ($2.2 < l/w < 3.8$) can be explained geometrically by the shape of bounding faults induced by an initial deep stepover. Changes in basin shape with increasing strike-slip displacement cause only slight modifications to this ratio.

4. For large displacements, a horsetail splay can develop in the vicinity of the intersection between transform and divergent boundaries. Within the horsetail splay, block rotations about vertical and horizontal (tilting) axes lead to the formation of a surface slope perpendicular to the slope of the divergent basin. This mechanism can explain at least partly the formation of tilted marginal ridges at transform margins.

Acknowledgements

Thanks are due to P. Allemand, J.F. Ballard and J.J. Kermarec for their help in carrying out experiments, and M.S.N. Carpenter who improved the English style. D. Bahat is thanked for a helpful review.

References

Allemand, P., Brun, J.P., Davy, P., Van Den Driessche, J., 1989. Symétrie et asymétrie des rifts et mécanismes d'amincissement de la lithosphère. Bulletin de la Société Geologique de France 8, 445–451.

Allemand, P., Brun, J.P., 1991. Width of continental rifts and rheological layering of the lithosphere. Tectonophysics 188, 63–69.

Aydin, A., Nur, A., 1982. Evolution of pull-apart basins and their scale independence. Tectonics 1, 91–105.

Aydin, A., Nur, A., 1985. The types and roles of stepovers in strike-slip tectonics. In: Biddle, K.T., Christie-Blick, N., (Ed.). Strike-slip deformation, basin formation, and sedimentation, 37. Society of Economic Paleontologists and Mineralogists, Special Publication, pp. 35–44.

Bahat, D., 1982. Extensional aspects of earthquake induced ruptures determined by an analysis of fracture bifurcation. Tectonophysics 83, 163–183.

Bahat, D., 1983. New aspects of rhomb structures. Journal of Structural Geology 5, 591–601.

Bartlett, W.L., Friedman, M., Logan, J.M., 1981. Experimental folding and faulting of rocks under confining pressure. Part IX: wrench faults in limestone layers. Tectonophysics 79, 255–277.

Basile, C., 1990. Analyse structurale et modélisation analogique d'une marge transformante: l'exemple de la marge profonde de Côte d'Ivoire–Ghana, 39. Mémoires et Documents du CAESS Rennes.

Basile, C., Mascle, J., Popoff, M., Bouillin, J.P., Mascle, G., 1993. The Ivory Coast–Ghana transform margin: a marginal ridge structure deduced from seismic data. Tectonophysics 222, 1–19.

Ben-Avraham, Z., 1985. Structural framework of the Gulf of Elat (Aqaba), northern Red Sea. Journal of Geophysical Research 90, 703–726.

Ben-Avraham, Z., Ten Brink U., 1989. Transverse faults and segmentation of basins within the Dead Sea Rift. Journal of African Earth Sciences 8, 603–616.

Byerlee, J., 1978. Friction of rocks. Pure and Applied Geophysics 116, 615–626.

Christie-Blick, N., Biddle, K.T., 1985. Deformation and basin formation along strike-slip faults. In: Biddle, K.T., Christie-Blick N., (Ed.). Strike-slip deformation, basin formation, and sedimentation, 37. Society of Economic Paleontologists and Mineralogists, Special Publication, pp. 1–35.

Cobbold, P.R., Brun, J.P., Davy, P., Fiquet, G., Basile, C., Gapais, D., 1989. Some experiments on block rotation in the brittle upper crust. In: Kissel, C., Lag C., (Ed.). Paleomagnetic rotations and continental deformation, NATO ASI Series C 254, pp. 145–155.

Davy, P., Cobbold, P.R., 1991. Experiments on shortening of a 4-layer model of the continental lithosphere. Tectonophysics 188, 1–25.

Delteil, J.R., Valery, P., Montadert, C., Fondeur, C., Patriat, P., Mascle, J., 1974. Continental margin in the northern part of the gulf of Guinea. In: Burk, C.A., Drake C.L., (Ed.). Geology of continental margins. Springer, New York, pp. 297–311.

Dooley, T., McClay, K., 1997. Analog modeling of pull-apart basins. American Association of Petroleum Geologists Bulletin 81, 1804–1826.

Emmons, R.C., 1969. Strike-slip rupture pattern in sand models. Tectonophysics 7, 71–87.

Eyal, Y., Eyal, M., Bartov, Y., Steinitz, G., Folkman, Y., 1986. The origin of the Bir Zreir rhomb-shaped graben, eastern Sinai. Tectonics 5, 267–277.

Faugère, E., Brun, J.P., Van Den Driessche, J., 1986. Bassins asymétriques en extension pure et en décrochement: modèles expérimentaux. Bulletin des Centres de Recherche et d'Exploration–Production Elf Aquitaine 10, 13–21.

Fox, P.J., Gallo, D.G., 1984. A tectonic model for ridge–transform–ridge plate boundaries: implications for the structure of oceanic lithosphere. Tectonophysics 104, 205–242.

Freund, R., 1974. Kinematics of transform and transcurrent faults. Tectonophysics 21, 93–134.

Freund, R., Zak, I., Garfunkel, Z., 1968. Age and rate of the sinistral movement along the Dead Sea Rift. Nature 220, 253–255.

Grant, A.C., 1977. Multichannel seismic reflection profiles of the continental crust beneath the Newfoundland Ridge. Nature 270, 22–25.

Heimann, A., Eyal, M., Eyal, Y., 1990. The evolution of Barahta rhomb-shaped graben, Mount Hermon, Dead Sea Transform. Tectonophysics 180, 101–110.

Hempton, M.R., Neher, K., 1986. Experimental fracture, strain and subsidence patterns over en échelon strike-slip faults: implications for the structural evolution of pull-apart basins. Journal of Structural Geology 8, 597–605.

Hubbert, M.K., 1951. Mechanical basis for certain familiar geologic structures. Geological Society of America Bulletin 62, 355–372.

Johnson, C.E., Hadley, D.M., 1976. Tectonic implications of the Brawley earthquake swarm, Imperial Valley, California, January 1975. Bulletin of the Seismological Society of America 66, 1133–1144.

Jolivet, L., Huchon, P., Brun, J.P., Le Pichon, X., Chamot-Rooke, N., Thomas, J.C., 1991. Arc deformation and marginal basin opening: Japan Sea as a case study. Journal of Geophysical Research 96, 4367–4384.

Kashai, E.L., Croker, P.F., 1987. Structural geometry and evolution of the Dead Sea–Jordan rift system as deduced from new subsurface data. Tectonophysics 141, 33–60.

Mandl, G., 1988. Mechanics of Tectonic Faulting: Models and Basic Concepts. Elsevier, Amsterdam.

Mandl, G., De Jong, L.N.J., Maltha, A., 1977. Shear zones in granular material. Rock Mechanics 9, 95–144.

Mann, P., Hempton, M.R., Bradley, D.C., Burke, K., 1983. Development of pull-apart basins. Journal of Geology 91, 529–554.

Manspeizer, W., 1985. The Dead Sea Rift: impact of climate and tectonism on Pleistocene and Holocene sedimentation. In: Biddle, K.T., Christie-Blick, N., (Ed.). Strike-slip deformation, basin formation, and sedimentation, 37. Society of Economic Paleontologists and Mineralogists, Special Publication, pp. 143–158.

Mascle, J., Blarez, E., 1987. The Ivory-Coast–Ghana continental margin: a model for transform margin evolution. Nature 326, 378–381.

Mauduit, T., Dauteuil, O., 1996. Small-scale models of oceanic transform zones. Journal of Geophysical Research 101, 20,195–20,209.

McClay, K., Dooley, T., 1995. Analogue models of pull-apart basins. Geology 23, 711–714.

Nalpas, T., Brun, J.P., 1993. Salt flow and diapirism related to extension at crustal scale. Tectonophysics 228, 349–362.

Naylor, M.A., Mandl, G., Sijpesteijn, C.H.K., 1986. Fault geometries in basement-induced wrench faulting under different initial stress states. Journal of Structural Geology 8, 737–752.

Rodgers, D.A., 1980. Analysis of pull-apart basin development produced by en échelon strike-slip faults. In: Balance, P.F., Reading, H.G., (Ed.). Sedimentation in oblique-slip mobile zones, 4. International Association of Sedimentologists Special Publication, pp. 27–41.

Scrutton, R.A., 1976. Crustal structure at the continental margin of South Africa. Geophysical Journal of the Royal Astronomical Society 44, 601–623.

Segall, P., Pollard, D.D., 1980. Mechanics of discontinuous faults. Journal of Geophysical Research 85, 4337–4350.

Sylvester, A.G., 1988. Strike-slip faults. Geological Society of America Bulletin 100, 1666–1703.

Tchalenko, J.S., 1970. Similarities between shear zones of different magnitudes. Geological Society of America Bulletin 81, 1625–1640.

Tchalenko, J.S., Ambraseys, N.N., 1970. Structural analysis of the Dasht-e Bayaz (Iran) earthquake fractures. Geological Society of America Bulletin 81, 41–60.

Tron, V., Brun, J.P., 1991. Experiments on oblique rifting in brittle–ductile systems. Tectonophysics 188, 71–84.

Zak, I., Freund, R., 1981. Asymmetry and basin migration in the Dead Sea Rift. Tectonophysics 80, 27–38.

Zhang, P., Burchfiel, B.C., Chen, S., Deng, Q., 1989. Extinction of pull-apart basins. Geology 17, 814–817.